Applied Surface Science 669 (2024) 160585

Contents lists available at ScienceDirect

Applied Surface Science

journal homepage: www.elsevier.com/locate/apsusc

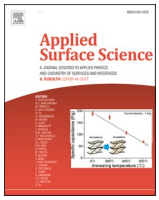

Full Length Article

Understanding the passivation layer formed by tolyltriazole on copper, bronze, and brass surfaces

Alexander J. Rossin [a], Federico Grillo [a], Stephen M. Francis [a], David N. Miller [a,1], Andrew K. Rossall [b], Jakob A. van den Berg [b], Gregory J. Hunt [c], Christopher J. Baddeley [a,*]

[a] EaStCHEM - School of Chemistry, University of St Andrews, St Andrews KY16 9ST, UK
[b] Ion Beam Centre, School of Computing and Engineering, University of Huddersfield, Huddersfield HD1 3DH, UK
[c] Strategic Research, Lubrizol Limited, Nether Lane, Hazelwood DE56 4AN, UK

ARTICLE INFO

Keywords:
Copper alloys
Corrosion
Tolytriazole
MEIS
XPS
FIB
STEM
EDS

ABSTRACT

Tolyltriazole (TTAH) is used industrially as a corrosion inhibitor for copper alloys, particularly in organic media. In this study, the morphology and chemistry of the layer formed by TTAH on copper and copper alloys under realistic conditions is investigated, with focus on the effects due to the presence of tin or zinc in the substrates. A combination of X-ray photoelectron spectroscopy (XPS), medium energy ion scattering (MEIS), and scanning transmission electron microscopy (STEM) has been used. It was found that an inhomogeneous metal–organic layer forms on the surface of copper specimens, likely in the form of copper nanoparticles surrounded by Cu_xTTA_y complexes. This layer increases in thickness for at least 30 days. Chemically, the copper species in the layer are initially in the +2 oxidation state, but after longer exposure to TTAH, mostly Cu(I) is observed. In bronze samples, tin does not appear to segregate to the surface layer. In brass samples, zinc is depleted from the bulk and forms a thicker Zn_xTTA_y layer.

1. Introduction

The favourable mechanical, thermal, and electrical properties of copper and its alloys make them well suited for a wide range of applications, including wiring, bearings, and fasteners. In comparison to steels, copper-based alloys exhibit good corrosion resistance. However, under harsh conditions – high temperature, extreme pH, ionic solutions – corrosion does occur, and often limits the lifetime of copper-alloy items. A method for combating this is to use molecular corrosion inhibitors [1]. Benzotriazole and its derivatives have been used for over half a century for this purpose [2–4]. In particular tolyltriazole (TTAH, Scheme 1) – as a mixture of 4- and 5-methyl-1H-benzotriazole – is used commonly because it is both highly effective and economical [5–14].

Triazole corrosion inhibitors function by adsorbing on the surface, and complexing with metal atoms mostly *via* the nitrogen atoms of the aromatic heterocycle to form a protective passivation layer [1,15–18]. During this process, the triazole loses its acidic proton to form an anion – in the case of TTAH we shall call the anion TTA^-. On copper specimens, since copper can be oxidised to both Cu(I) and Cu(II) compounds, in principle a variety of Cu_xTTA_y complexes is possible. As a comparison, in the case of BTAH (benzotriazole), it has been found that $Cu(I)_xBTA_y$ complexes usually form, most commonly $Cu(I)BTA_2$ [16,19–22], but Cu(II) can also be present under some conditions [19,22]. The details of the chemical structures formed vary considerably depending on the experimental conditions, and are a matter of active research [16–18,20–25].

Most of the work investigating copper corrosion inhibitors has been done using pure copper substrates, including with TTAH [6,8,9,26]. However, brass and bronze alloys are much more common in real applications. Therefore, it is important to investigate how the protective passivation layer is affected by the presence of other metals. Additionally, studies of BTAH and its derivatives are usually done in an aqueous medium [5–10] or in ultra-high vacuum [15–18,20,21,27,28], but TTAH in particular is often used in organic media, for example in automotive gear oil and automatic transmission fluid [29,30]. These corrosion concerns also exist for electrified vehicles [31,32]. Therefore, investigating the TTAH with materials used in gear boxes/transmissions

* Corresponding author.
E-mail address: cjb14@st-andrews.ac.uk (C.J. Baddeley).
[1] Present address: Energy Storage Research Group, School of Chemistry and Physics, Faculty of Science, Queensland University of Technology (QUT), Brisbane, Queensland 4001, Australia.

https://doi.org/10.1016/j.apsusc.2024.160585
Received 8 April 2024; Received in revised form 31 May 2024; Accepted 21 June 2024
Available online 22 June 2024

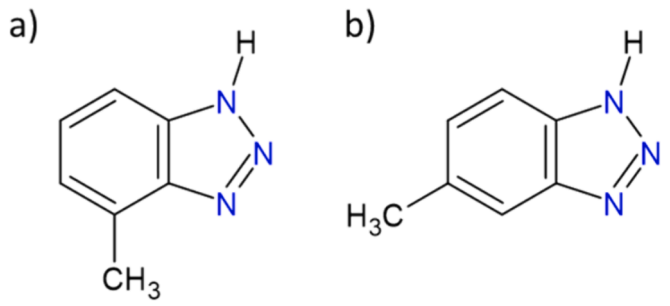

Scheme 1. Chemical structure of TTAH (4- and 5-Me-1H-benzotriazole).

and in an organic matrix is of utmost importance.

In this study, a combination of different analytical techniques was used to analyse copper, bronze, and brass surfaces that had been treated with TTAH in an organic medium, namely *n*-heptane, obtaining chemical and morphological information from the surface layers down to the bulk of the samples. Industrially common alloys and an elevated temperature were used to approximate realistic conditions. XPS shows the average composition and oxidation states of the elements of the very top surface layers of the samples; MEIS gives information about the composition depth profile up to a depth of around 20 nm; and cross-sectional STEM shows highly localised composition and morphology up to several hundred nm deep. This allowed the structure and chemistry of the passivation layer to be probed. The effects caused by the presence of zinc or tin were also observed, along with the effects of varied treatment times.

2. Material and methods

2.1. X-ray photoelectron spectroscopy (XPS)

XPS measurements were collected on a Scienta ESCA 300 spectrometer, using a SPECS Focus 600 monochromated Al K_α source (1486.6 eV, 12 kV, 200 W), operating at a base pressure of ca. 1×10^{-9} mbar. The detection system consisted of a large hemispherical analyser coupled to a multi-channel plate/video camera (base pressure ca. 5×10^{-10} mbar). The BE scale was calibrated to the C 1s line (285 eV). Data analysis was done using the CasaXPS software package [33].

2.2. Medium energy ion scattering (MEIS)

MEIS data were collected using the facility at the University of Huddersfield, using a nominally 100 keV He^+ beam with an incidence angle of 35.3°. Scattered ions were analysed using a toroidal electrostatic energy analyser, which allows simultaneous data collection over a range of energies (1.8 % pass energy) and angles (27°). The resulting two-dimensional tiles were combined digitally, and a spectrum at a scattering angle of 125.3° was extracted. Because the samples are polycrystalline in nature, channelling and blocking effects are averaged over all directions and therefore not considered of major importance.

2.3. Scanning transmission electron microscopy (STEM)

Samples for scanning transmission electron microscopy (STEM) were prepared by an in-situ focused ion beam lift out technique using a Scios Dualbeam focused ion beam scanning electron microscope (FIBSEM). The surface of the sample was protected by electron deposited carbon and platinum layers prior to ion milling, lift out and ion polishing (see SI1). STEM analysis was carried out using a probe-corrected Titan Themis operating at 200 kV equipped with SuperX windowless EDX detector.

2.4. Preparation of samples

Copper (half hard, 99.9 % pure, 0.5 mm foil), brass (half hard, 63 % Cu, 37 % Zn, 0.5 mm foil) and bronze (half hard, 94 % Cu, 6 % Sn, 0.5 mm foil) were purchased from Goodfellow and cut into ca. 1×1 cm^2 samples. *n*-Heptane and acetone were purchased from Fisher Scientific, and TTAH was provided by Lubrizol. The TTAH was determined to be a mixture of ca. 41 % and 59 % 4- and 5-methyl-1H-benzotriazole respectively, using 1H NMR (see SI2). Before treatment, samples were sonicated in acetone followed by *n*-heptane for 6 min each, then were placed in an autoclave with either pure *n*-heptane, or saturated (at room temperature) TTAH in *n*-heptane for 1, 3, 10, or 30 days at 130 °C; this temperature was chosen to approximate conditions in automobile applications. After treatment, samples were rinsed with *n*-heptane.

3. Results

3.1. XPS

Fig. 1 shows the Cu $2p_{3/2}$ region of the XP spectra for copper, brass and bronze samples that were sonicated in acetone and *n*-heptane, and then treated in *n*-heptane with TTAH for 1, 3, 10, and 30 days, compared with reference samples of the same metals/alloys sonicated in acetone and *n*-heptane only (further referred as "untreated" samples). On the untreated substrates, three distinct peaks can be seen, which have been labelled A1, A2, and B in Fig. 1, according to the notation introduced by Biesinger *et al.* [34,35] Peak A2 is located at 932.4, 931.9, and 932.3 eV for copper, bronze, and brass respectively. Since the BE of the Cu $2p_{3/2}$ core level peaks of Cu(0) and Cu(I) are very similar [36–38] peak A2 cannot be used reliably to identify whether Cu(0) or Cu(I) is present. However, the Cu $L_3M_{4,5}M_{4,5}$ Auger transitions of Cu(0) and Cu(I) are different in shape and occur at different kinetic energies. Specifically, the maxima of the most intense components for Cu(I) and Cu(II) are both at lower kinetic energy than for Cu(0) [35,36]. Fig. 2a–c shows the Cu $L_3M_{4,5}M_{4,5}$ Auger transitions for each sample. Fig. 2d shows a copper Wagner plot for the samples.

Peaks A1 and B correspond to the core-level peak and shake-up satellite from Cu(II) respectively [34]. B is observed at 934.9 eV for copper, and 934.7 eV for bronze and brass. B is broad, containing at least two components, and has a maximum in the range of 941–945 eV. Full peak fittings are provided in SI3.1.

Since the shake-up satellite is only present for Cu(II), it can be used to estimate the fraction of the total observed copper signal originated from species in the 2+ oxidation state. This is done by comparing the relative size of B and A1 + A2 to a pure Cu(II) compound as described by Biesinger *et al.* [34,35] In this work, a CuO spectrum measured on the same XPS instrument was used as the pure Cu(II) reference (SI3.1.1). These results are combined with Zn $2p_{3/2}$ and Sn $3d_{5/2}$ XPS data to give a comprehensive breakdown of the total metal signal, which is shown in Table 1 and Fig. 3 (Sn $3p_{5/2}$ and Zn $2d_{3/2}$ spectra and peak fitting are reported in SI3.2 and 3.3 respectively.).

In the untreated copper sample (Fig. 1a, black curve), 40 % of the copper signal is assigned to Cu(II); the remainder is assigned to Cu(I) from its location on the Wagner plot (Fig. 2d). However, the various contributions to the Auger peak cannot be separated, and it is possible that also some Cu(0) is present, and the lower kinetic energy of the primary peak in these samples is due to the contribution of the Cu(II) component. After treatment with TTAH for 24 h, peak A2 is greatly reduced, with the Cu(II) component comprising 86 % of the total copper signal (Fig. 1a, red curve). Over the course of the treatment, the intensity of peak A2 increases and peaks A1 and B decrease, with 70 % Cu(II) observed after 3 days (Fig. 1a, green curve), and no detectable Cu(II) signal observed after 10 days and 30 days (Fig. 1a, cyan and blue curves). The absence of the satellite structure (B) makes the absence of Cu(II) particularly clear since peak B is well separated from peak A2. The Wagner plot (Fig. 2d) shows that the kinetic energy of the Auger

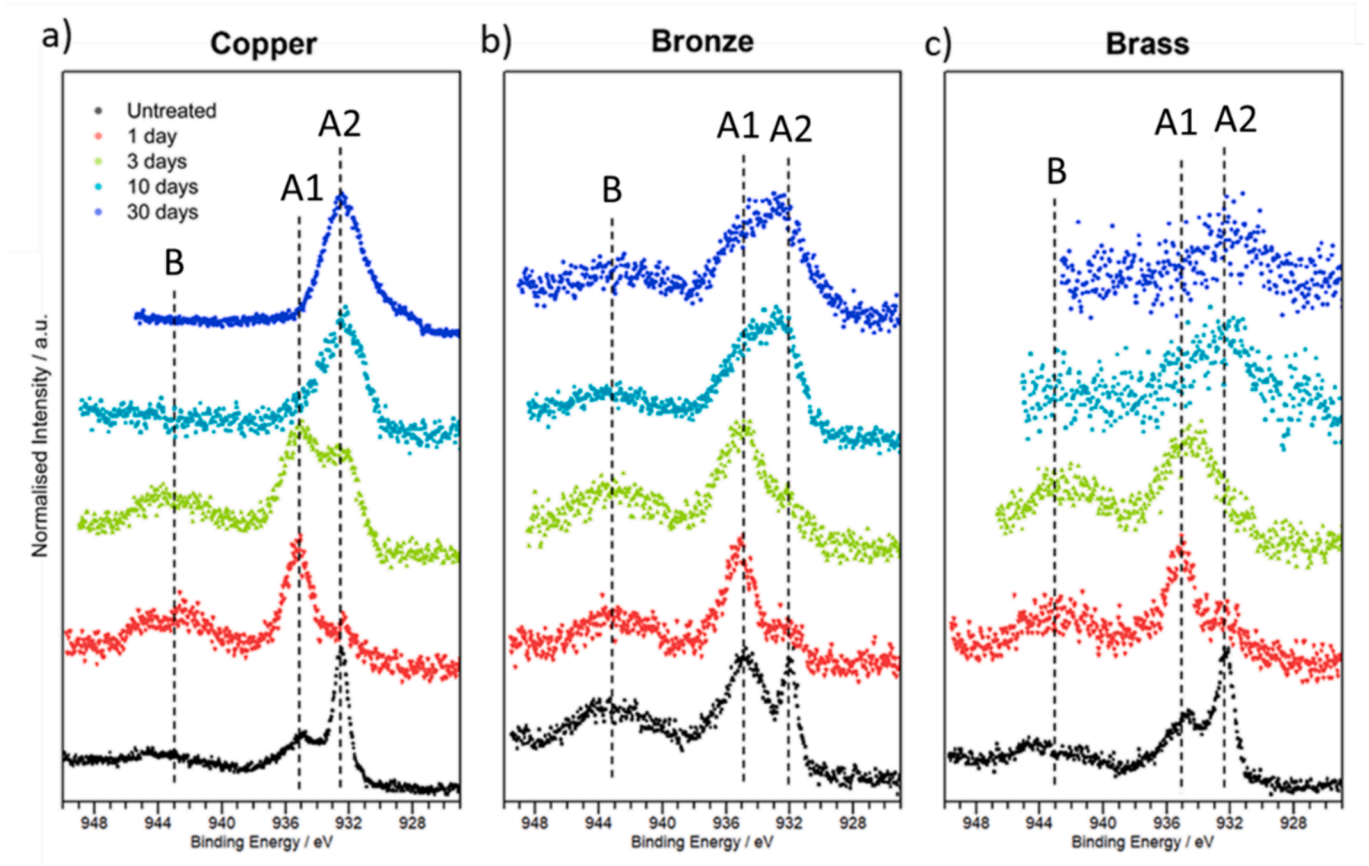

Fig. 1. Cu $2p_{3/2}$ XP spectra of copper, bronze, and brass samples in *n*-heptane treated with TTAH for 1–30 days, compared to untreated reference samples. Peak A2 corresponds to Cu(0) and/or Cu(I); peaks A1 and B correspond to Cu(II) core level and Cu(II) shake-up respectively.

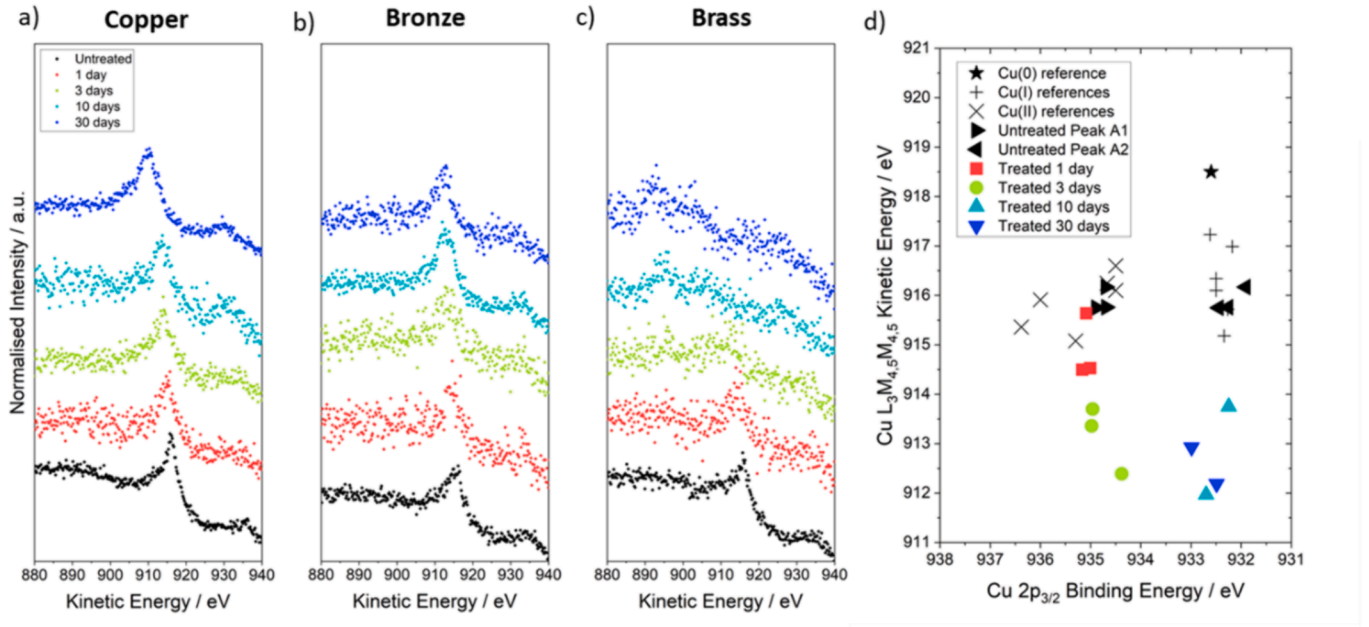

Fig. 2. (a–c) Cu $L_3M_{4,5}M_{4,5}$ Auger transitions of copper, bronze and brass samples in *n*-heptane treated with TTAH for 1–30 days, compared with untreated references samples. With the brass samples, the Cu and Zn $L_3M_{4,5}M_{4,5}$ Auger transitions partially overlap; in the samples treated for 3, 10, and 30 days, the weaker Cu signal is substantially obscured by the more intense Zn signal. (d) Cu Wagner plot; for the untreated samples, the binding energies of peak A1 and A2 are shown separately. For the treated samples only the most intense Cu $2p_{3/2}$ peak is shown.

Table 1
Metallic surface composition of copper, brass and bronze samples treated with TTAH for 1, 3, 10 and 30 days, compared to untreated reference samples. All values are a fraction of the total metal detected.

Preparation		Cu(0) + Cu(I)/%	Cu(II)/%	Zn/%	Sn/%
Copper	Untreated	60	40		
	1 day	14	86		
	3 days	30	70		
	10 days	100	0		
	30 days	100	0		
Bronze	Untreated	21	73		6.0
	1 day	17	83		
	3 days	22	78		
	10 days	58	42		
	30 days	65	35		
Brass	Untreated	33	32	34	
	1 day	10	80	10	
	3 days	10	36	54	
	10 days	21	0	79	
	30 days	9.2	0	91	

transition (Fig. 3a) is too low to indicate the presence of Cu(0), which is consistently reported at 918–919 eV;[36] this allows one to determine that peak A2 in the treated samples represents Cu(I).

On the bronze substrate a similar trend is observed, but with relatively more Cu(II) present throughout. Cu(II) accounts for ca. 73 % of the total metal signal in the untreated bronze sample (Fig. 1b, black curve). After 1 day of treatment with TTAH (Fig. 1b, red curve), the Cu(II) signal is increased to ca. 86 %. Over the course of the treatments, the relative amount of Cu(II) observed gradually decreases to 78 %, 42 %, and 35 % after 3, 10 and 30 days respectively. (Fig. 1b, green, cyan, and blue curves). In the untreated bronze sample, 6 % tin is observed – this is in line with the nominal composition of the alloy. The Sn $3d_{5/2}$ peak has a binding energy of 486.4 eV (SI3.2), indicating that tin is oxidised; [36,37] however, the binding energies of Sn(II) and Sn(IV) have overlapping ranges, 486–487 eV, therefore a more accurate attribution cannot be made at this point. No tin signal was observed for any of the treated samples (SI3.2).

On the brass samples, the trend in copper oxidation state is very similar to that obtained for the copper samples. In the untreated sample (Fig. 1c, black curve), 32 % of the total metal signal is originated from Cu(II) and 33 % from Cu(I) and/or Cu(0)); 34 % zinc is measured – in line with the nominal composition of the alloy. The Zn $2p_{3/2}$ has a binding energy of 1021.9 eV (SI 3.3) compatible with the presence of metallic zinc. With treatment for 1 day (Fig. 1c, red curve), the Cu(II) signal is increased to 80 %, then the signal decreases to 36 % after 3 days (Fig. 1c, green curve); after 10 and 30 days (Fig. 1c, cyan and blue curves) no Cu(II) is detected. The signal from Cu(I) and/or Cu(0) is 10 % of the total metal signal after 1 and 3 days, 21 % after 10 days, and 9.2 % after 30 days. Additionally, there is a correlation between the relative intensity of the Zn $2p_{3/2}$ signal and the treatment time, as the amount of surface zinc is estimated to go from 10 % after 1 day up to 91 % after 30 days (SI3.3). The combined effect is that the total metallic signal detected by XPS goes from predominantly copper in the + 2 oxidation state after 1 day of treatment, to predominantly zinc after 30 days of treatment, with some Cu(I) observed throughout – particularly at intermediate treatment times (Fig. 3c). After treatments with TTAH, although charging effects due to the deposited layer cause peak broadening and asymmetry, the Zn $2p_{3/2}$ shifts to higher binding energies. This is compatible with oxidation to the +2 state.[39,40].

3.2. *MEIS*

Fig. 4 shows the MEIS spectra for copper, brass, and bronze samples treated with TTAH in *n*-heptane for 1, 3, 10, and 30 days compared with untreated samples of the same alloys. Copper and zinc edges cannot be differentiated due to the similarity in their atomic weights and give a combined signal with an edge at 81 keV. The tin edge is at 90 keV. The copper samples that have been treated with TTAH show a substantial decrease of the signal intensity at the copper edge, indicating a decrease in copper concentration at the surface. If the copper was simply being covered by other elements, the energy of the edge would be decreased without the low intensity plateau that is observed here. This decreased copper density can be explained as copper being diluted by light elements (e.g. C, N, O) that are not distinguished from the MEIS yield from higher masses, indicating the presence of a copper-organic layer. The depth of this effect is greater with longer treatment time. With the bronze substrate, the tin signal at the surface is no longer measurable after 1 day of treatment; the depth of this effect is also greater with longer treatment time, and the tin signal is suppressed by the copper signal in the samples treated for 10 and 30 days. Meanwhile, the copper edge exhibits behaviour similar to the pure copper sample, with a plateau that increases in depth with treatment time; this indicates the presence of a layer on top of the bulk copper with lower metal concentration, likely a copper-organic layer. In the brass the combined copper and zinc edge shows a similar plateau, indicating a layer with decreased total metal concentration at the surface; due to the similarity of the copper and zinc edges, it cannot be determined from these data whether this metal–organic layer contains copper, zinc or a combination of the two elements.

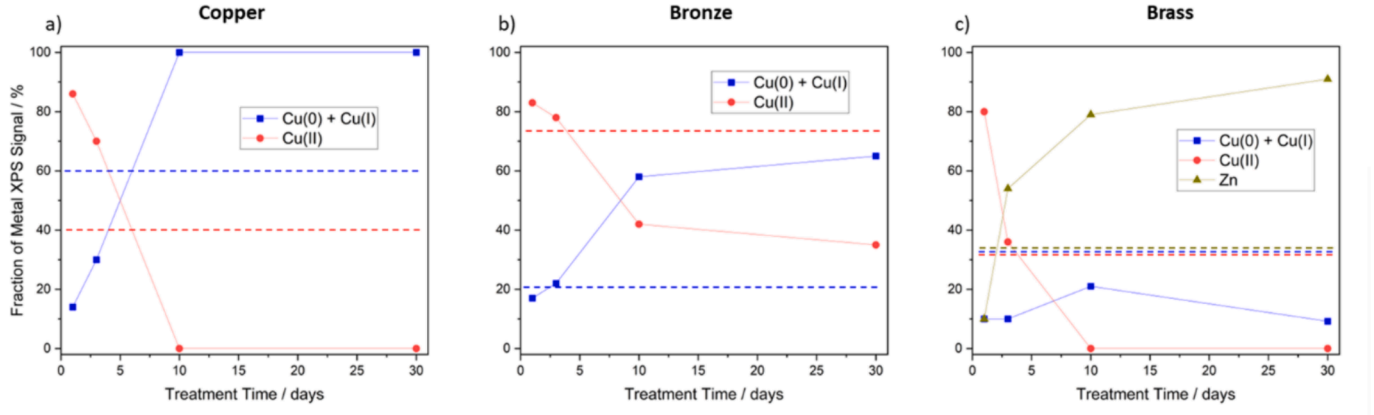

Fig. 3. Variation in the metal XPS signals on (a) copper, (b) bronze, and (c) brass samples treated with TTZL in *n*-heptane for 1–30 days. Dashed lines show the composition of untreated reference samples.

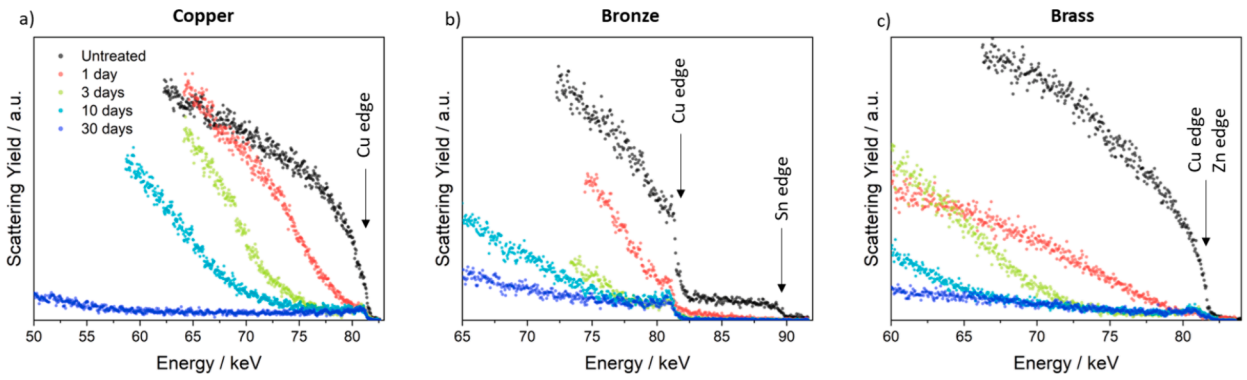

Fig. 4. MEIS spectra for (a) copper, (b) bronze, and (c) brass samples treated with TTAH for 1 to 30 days, compared to untreated reference samples.

3.3. STEM and EDS

STEM was done on cross-sections of the surfaces of copper, bronze, and brass samples treated for 30 days. The longest treated samples were used because they were determined from MEIS analysis to have the thickest M_xTTA_y surface layers build up, and larger scale features are more easily resolved in the microscopy.

A high-angle annular dark-field (HAADF) STEM image (Fig. 5a) from a cross-section of the surface of a copper sample treated in *n*-heptane with TTAH for 30 days shows a layer of lower density above the bulk. It can be seen from EDS (Fig. 5b, c, and d, additional details in SI4.1) that the majority of the signal in this layer comes from copper, but also some nitrogen is present. Nitrogen is a difficult element to detect with EDS because of its low density. Within this layer there are occasional brighter features, containing mostly copper.

Fig. 6a and c show HAADF STEM images of a cross-section of the surface of a bronze sample treated with TTAH in *n*-heptane for 30 days; Fig. 6b shows the EDS intensity of copper and tin along the arrow indicated in Fig. 6a, averaged across the entire width of the image. There is a layer of lower density above the bulk. Fig. 6d shows a magnification of the section of this layer indicated on Fig. 6c, alongside EDS maps of oxygen, copper, and tin (additional details are given in SI4.2). The upper part of this layer consists of rounded features roughly 5–20 nm in size, surrounded by even less dense material; EDS shows that this region contains copper, and the denser features are particularly copper-rich (though still at a much lower concentration than the bulk). These are likely to be copper nanoparticles, which do not appear as bright as the bulk because their average sizes are less than the thickness of the sample. The lower part of the surface layer – directly above the bulk – has a finer structure, and shows relatively less copper and more tin and oxygen.

Fig. 7a and b show HAADF STEM images from different areas of a cross-section of the surface of a brass sample treated with TTAH for 30 days. For *ca.* 20 nm above the bulk in both images, there is an inhomogeneous layer that looks similar to what is present on the copper and bronze samples (Figs. 5 and 6). Fig. 7d shows a magnification of this layer, with an EDS map of copper and zinc (additional details are given in SI4.3). This layer is rich in copper – particularly the denser spots – but also contains some zinc. Above this is a layer that appears more homogeneous, which varies in thickness from only a few nanometres (Fig. 7a) to *ca.* 300 nm (Fig. 7b). A detail of this layer is shown in Fig. 7b. As shown by comparing the elemental maps (Fig. 7d and e), the upper layer contains primarily zinc rather than copper. This layer shows copper-rich areas, which are much more sparse than in the lower layer. There is oxygen present at the interface between the bulk and the surface layer, especially in crevices (SI4.3). The top ca. 20 nm of the bulk shows much more copper relative to zinc than the rest of the bulk; this indicates a depletion of zinc at the interface (Fig. 7c).

3. Discussion

TTAH is widely used as a corrosion inhibitor on copper and copper alloys, specifically in organic solvents [29,30]. This is because the presence of the methyl group renders TTAH more soluble than BTAH in an organic medium. In order to understand better the operation of TTAH, and in particular how its corrosion-inhibiting performance changes depending on the presence of alloying elements, a series of experiments were carried out. This involved treatment of copper, brass, and bronze substrates at 130 °C with TTAH in *n*-heptane; an organic medium and elevated temperature were used to model applications in automotive transmission and gear oil.

Samples were analysed with a set of experimental techniques sensitive to different depths below the surface, with XPS being the most surface sensitive; MEIS allowing one to gather information up to around 20 nm deep; and cross-sectional STEM probing composition and morphology up to several hundred nm deep. The lack of literature on

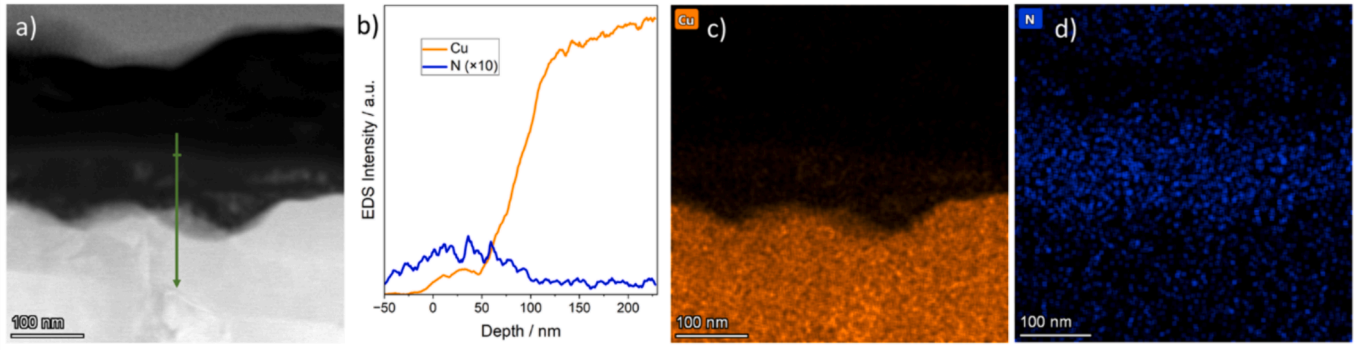

Fig. 5. (a) HAADF STEM image of a cross-section of the surface of a copper sample treated with ttah for 30 days. (b) EDS intensity of Cu and N along the indicated arrow in (a), averaged across the entire width of the image. (c) EDS map of Cu. (d) EDS map of N.

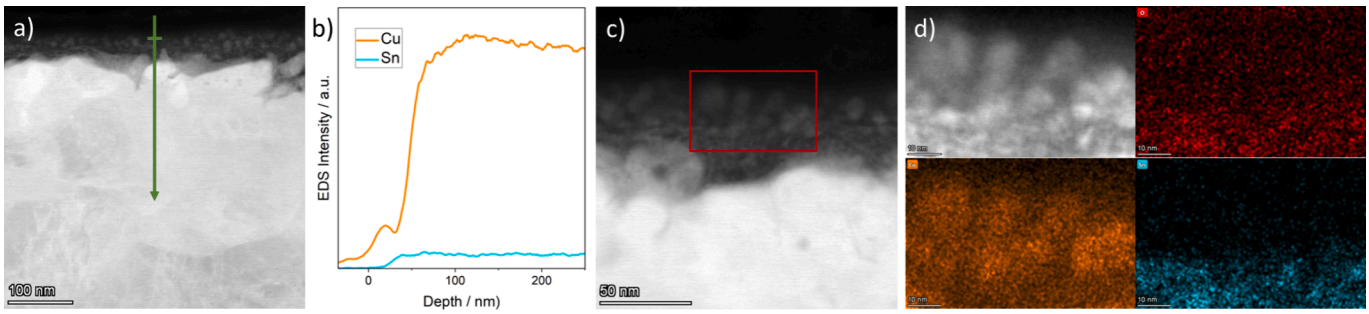

Fig. 6. STEM and EDS data from a cross-section of the surface of a bronze sample treated with TTAH for 30 days. (a) HAADF image. (b) EDS intensity for Cu and Sn along the arrow indicated in (a), averaged over the entire width of the image. (c) HAADF image. (d) HAADF image and O, Cu, and Sn EDS maps of the area indicated by the red rectangle in (b). (For interpretation of the references to colour in this figure legend, the reader is referred to the web version of this article.)

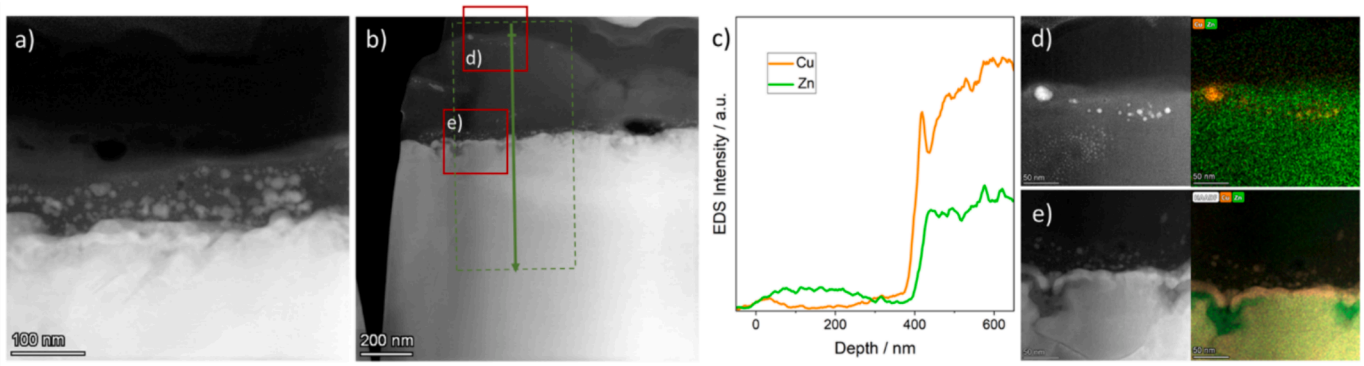

Fig. 7. (a) and (b) HAADF STEM images from a cross-section of the surface of a brass sample treated with TTAH for 30 days. (c) The EDS intensity along the indicated direction in (b), averaged across the indicated region. (d) and (e) Higher resolution HAADF images of the indicated regions in b), alongside EDS element maps of Cu and Zn.

TTAH prompted us to refer to papers on BTAH as a comparison; this is justified by the fact that theoretical studies have shown that a variety of azole compounds – including BTAH and TTAH – interact with copper and copper alloy surfaces in a similar manner, coordinating *via* two adjacent aromatic nitrogen atoms [41–46].

For the pure copper substrate, on initial exposure to TTAH in *n*-heptane, an increased Cu(II) signal relative to an untreated reference was observed *via* XPS. With longer treatment time, a decrease in the relative Cu(II) signal and a corresponding increase in Cu(I) was seen. This could be explained by the TTAH initially oxidising metallic copper to a kinetically favoured Cu(II) species, which subsequently is reduced to a thermodynamically favoured Cu(I) species. For example:

$$n\mathrm{Cu} + 2n\mathrm{TTAH} \rightarrow \mathrm{Cu(II)_nTTA_{2n}} + n\mathrm{H_2} (1)$$

$$\mathrm{Cu(II)_nTTA_{2n}} + \mathrm{nCu} \rightarrow \mathrm{Cu(I)_{2n}TTA_{2n}} (2)$$

An alternative interpretation is that Cu(II) species form from a reaction between the TTAH and already-present surface compounds (oxides, hydroxides, etc.), whereas Cu(I) forms in the absence of these compounds. For example, if Cu(I) oxide is present, this could be oxidised by the addition of TTAH to a Cu(II) species, shown in Eq. (3). Once the pre-existing species are exhausted, the dominant process becomes the oxidation of metallic copper to Cu(I), for example as shown in Eq. (4).

$$\mathrm{Cu(I)_2O} + 2\mathrm{TTAH} \rightarrow \mathrm{Cu(II)_2O(TTA)_2} + \mathrm{H_2} (3)$$

$$2n\mathrm{Cu} + 2n\mathrm{TTAH} \rightarrow \mathrm{Cu(I)_{2n}TTA_{2n}} + n\mathrm{H_2} (4)$$

If the formation of Cu(II) occurred after treatment by oxidation from exposure to atmosphere due to transferring the samples between the autoclave and analysis instruments, it would be expected to either be observed in all treated samples (if the surface layer is being oxidised) or in the samples not treated with TTAH (if it was happening through the layer). Because neither of these scenarios are observed, it is unlikely that the formation of Cu(II) is due to atmospheric oxidation after treatment. For example, it was shown that BTAH can inhibit atmospheric oxidation of brass up to 500 °C [47].

The initial prevalence of Cu(II) is different to what has generally been reported for BTAH in the literature, where Cu(I) species are formed very quickly, with little evidence of Cu(II) [3,19–21]. This difference could be caused by TTAH behaving differently to BTAH, however this is unlikely since a methyl group is only weakly electron donating and its purpose is mainly to increase solubility in organic solvents. In fact, it has been reported that adsorption of both BTAH and TTAH on Cu(1 1 1) should occur through the triazole moiety [41]. It is also possible that the difference in observations is because studies of BTAH were done using an aqueous medium, while the present research was done in an organic medium. Specifically, if Cu(II) compounds are initially produced with the participation of pre-existing surface species (i.e. Eq. (3)), and these compounds are more polar than the predominant Cu(I) compounds, then they could persist on the surface for a longer time in a non-polar organic medium than in an aqueous medium.

In one previous study where a CuCl surface was treated with BTAH, it was found that a small amount of Cu(II) was present after 30 min of treatment, but no Cu(II) was detectable after 120 min of treatment [22]. This could be a similar chemical process of pre-existing CuCl being oxidised to Cu(II), however the non-polar *n*-heptane medium used in the present work causes these species to persist on the surface for longer times. Quantitative analysis of the XPS data (see SI 3.8) indicates TTA:Cu ratios between 1 and 4, consistent with $\mathrm{Cu_xTTA_y}$ being the primary component of the surface layer; as a comparison, previous studies have found a BTA:Cu ratio of 1 or 2 for surface species [15–18,48].

MEIS revealed the presence of a surface layer with a decreased

density of copper, interpreted as a metal–organic layer; light elements – such carbon, oxygen, and nitrogen – are not observed directly by MEIS. The thickness of this layer continues to grow through at least 30 days of treatment. Cross-section STEM of the sample treated for 30 days shows a surface layer that is roughly 40–60 nm thick, consisting of occasional copper nanoparticles surrounded by a homogenous matrix with a low level of copper, presumably Cu_xTTA_y species.

On the bronze samples, XPS measurements show that the trend in surface copper oxidation state is similar to that observed for the pure copper substrate, with mostly Cu(II) present after 1 day of treatment and the relative amount of Cu(I) increasing after that. However, unlike for the pure copper surface, a substantial amount of Cu(II) is present on all samples, constant at around 50 % of total copper signal after both 10 and 30 days. On the untreated bronze reference sample, around 6 % of the total XPS metal signal is originated from tin. Roughly this is in line with the nominal composition of the bronze. In all treated samples, no tin signal was observed; additionally, no tin EDS signal was observed in the upper half of the surface layer in the STEM sample. Quantitative analysis of XPS indicates (S3.8) TTA:Cu ratios between 1.5 and 3, consistent with Cu_xTTA_y being the primary component of the surface layer, and similar to the BTA:Cu ratios of 1 or 2 found in previous studies [15–18,48].

The MEIS data for the bronze samples show a trend of increasing thickness of the passivation layer similar to that recorded for the copper samples. The tin edge for treated samples is shifted to from *ca*. 90 eV in the untreated reference, to *ca*. 85 eV after 1 day of treatment, and low enough to be hidden by the copper edge (*ca*. 82 eV) after longer treatment. This indicates that no observable tin is present at the surface, in agreement with the XPS and STEM. While the lower tin edge is visible in the samples treated for 1 and 3 days, it is completely suppressed by the copper edge for samples treated for 10 and 30 days. Cross-sectional STEM of the sample treated for 30 days shows a slightly thinner layer of about 30–50 nm. Notably, there is a much higher concentration of structures attributed to nanoparticles, which are densely packed without large areas of the homogeneous layer between them. While no tin is observed in the upper part of the layer (in agreement with XPS and MEIS observations), increased tin and oxygen contents are observed in the lower part of the layer. This can be interpreted as tin oxide present between the Cu_xTTA_y passivation layer and the bulk alloy, as a consequence of TTAH selectively segregating copper to the surface layer [21].

On the untreated brass reference sample, around 31 % of the total XPS metal signal is originated from zinc, roughly in line with the bulk composition. Upon treatment with TTAH for 1 day, this decreases to 9 %; on further treatment it increases progressively to reach around 86 % after 30 days. Quantitative analysis of XPS (SI3.8) indicates TTA:M ratios between 1.5 and 2.5, consistent with M_xTTA_y being the primary component of the surface layer, and similar to the BTA:Cu ratios of 1 or 2 found in previous studies [15–18,48].

In the MEIS data from the brass samples, the combined copper and zinc edges show a similar behaviour to the copper edge in the data from the copper samples, indicating the presence of a metal organic layer. Because the copper and zinc edges are similar in energy, MEIS cannot be used to distinguish between these elements. By STEM and EDS it is observed that after 30 days the layer is copper-rich near the bulk, and becomes more and more zinc-rich moving towards the surface. Additionally, the layer produced after 30 days of treatment in TTAH is much thicker than that obtained on copper or bronze samples, at around 200 nm; the top of the bulk is notably depleted of zinc. This leads to the interpretation that the reaction of copper with TTAH happens more quickly than the reaction with zinc. Then in the long run the passivation layer that is formed is ineffective at blocking the transport of zinc atoms thought the Cu_xTTA_y layer, leading to a thick Zn_xTTA_y layer forming over the Cu_xTTA_y layer. As a comparison, migration of copper atoms from the bulk to the surface layer [21] layer is one of the proposed mechanisms for the growth of the Cu_xBTA_y layer on oxidised copper [49]. This indicates that the layer formed by TTAH on alloys containing zinc is not as effective at inhibiting corrosion as the layer formed on alloys without zinc.

4. Conclusions

When copper, brass, or bronze is treated with TTAH in *n*-heptane at elevated temperature, a metal–organic (M_xTTA_y) layer forms. This layer is highly inhomogeneous and is best described as copper nanoparticles surrounded by Cu_xTTA_y species. The thickness of the metal–organic layer grows for at least 30 days. Over this time period, the copper surface atoms change oxidation state from predominately Cu(II) to predominantly Cu(I). When tin is present in the alloy, it is not involved in the M_xTTA_y layer, but there is tin oxide between the layer and the bulk. When zinc is present, a thicker, more homogeneous Zn_xTTA_y layer forms over the predominantly Cu_xTTA_y layer. This study shows that there are considerable implications for the use of TTAH as a corrosion inhibitor for copper alloys: TTAH seems likely effective on protecting bronze in a manner similar to pure copper, whereas on brass it is less effective since it appears that zinc can relatively easily be transferred through the Cu_xTTA_y layer and be depleted from the underlying surface.

CRediT authorship contribution statement

Alexander J. Rossin: Writing – review & editing, Writing – original draft, Visualization, Investigation, Data curation, Conceptualization. **Federico Grillo:** Writing – review & editing, Supervision, Investigation, Funding acquisition, Data curation, Conceptualization. **Stephen M. Francis:** Investigation, Data curation. **David N. Miller:** Investigation, Data curation. **Andrew K. Rossall:** Investigation, Data curation. **Jakob A. van den Berg:** Investigation, Data curation. **Gregory J. Hunt:** Supervision, Funding acquisition, Conceptualization. **Christopher J. Baddeley:** Writing – review & editing, Supervision, Project administration, Funding acquisition, Conceptualization.

Declaration of competing interest

Alexander J. Rossin reports financial support was provided by Lubrizol Ltd. The other authors declare that they have no known competing financial interests or personal relationships that could have appeared to influence the work reported in this paper.

Data availability

The research data underpinning this publication can be accessed at https://doi.org/10.17630/b9356343-1e42-4fcc-b878-8c31f4823e94.

Acknowledgements

Lubrizol Ltd. is acknowledged for funding (AJR) and supplying TTAH. EPSRC is acknowledged (EP/L017008/1, EP/T019298/1, EP/R023751/1) for electron microscopy. James Bird and Robert Calmer from Lubrizol Ltd. are acknowledged for assistance with the compositon of the graphical abstract.

Appendix A. Supplementary material

Supplementary data to this article can be found online at https://doi.org/10.1016/j.apsusc.2024.160585.

References

[1] M.M. Antonijevic, M.B. Petrovic, Copper corrosion inhibitors. A review, Int. J. Electrochem. Sci 3 (2008) 1–28, https://doi.org/10.1016/S1452-3981(23)15441-1.

[2] N.K. Allam, A.A. Nazeer, E.A. Ashour, A review of the effects of benzotriazole on the corrosion of copper and copper alloys in clean and polluted environments, J. Appl. Electrochem. 39 (2009) 961–969, https://doi.org/10.1007/s10800-009-9779-4.

[3] M. Finšgar, I. Milošev, Inhibition of copper corrosion by 1,2,3-benzotriazole: a review, Corros. Sci. 52 (2010) 2737–2749, https://doi.org/10.1016/j.corsci.2010.05.002.

[4] Y.I. Kuznetsov, Triazoles as a class of multifunctional corrosion inhibitors. A review. part I. 1,2,3-benzotriazole and its derivatives. Copper, zinc and their alloys, Int. J. Corros. Scale Inhib. 7 (2018) 271–307. https://doi.org/10.17675/2305-6894-2018-7-3-1.

[5] C.J. Korpics, Aromatic triazoles as corrosion inhibitors of copper and copper alloys, Anti-Corros. Methods Mater. 21 (1974) 11–13, https://doi.org/10.1108/eb006943.

[6] R. Walker, Corrosion inhibition of copper by tolyltriazole, Corrosion 32 (1976) 339–341, https://doi.org/10.5006/0010-9312-32.8.339.

[7] T. Notoya, G.W. Poling, Benzotriazole and tolyltriazole as corrosion inhibitors for copper and brasses, Boshoku. Gijuts. 30 (1981) 381–389, https://doi.org/10.3323/jcorr1974.30.7_381.

[8] C. Törnkvist, D. Thierry, J. Bergman, B. Liedberg, C. Leygraf, Methyl substitution in benzotriazole and its influence on surface structure and corrosion inhibition, J. Electrochem. Soc. 136 (1989) 58–64, https://doi.org/10.1149/1.2096614.

[9] M.K. Hsieh, D.A. Dzombak, R.D. Vidic, Effect of tolyltriazole on the corrosion protection of copper against ammonia and disinfectants in cooling systems, Ind. Eng. Chem. Res. 49 (2010) 7313–7322, https://doi.org/10.1021/ie100384d.

[10] T. Yang, W. Chen, X. Li, J. Song, L. Dong, Y.Q. Fu, Environment-friendly and chromium-free passivation of copper and its alloys, Mater. Today Commun. 29 (2021) 102826, https://doi.org/10.1016/j.mtcomm.2021.102826.

[11] L. Broch, J.S. Crespo, L.V.R. Beltrami, M. Giovanela, Copper corrosion inhibition in acidic aqueous media through tolyltriazole application: performance analysis, Chem. Eng. Commun. (2024), https://doi.org/10.1080/00986445.2024.2344801.

[12] H.E. Fathabadi, M. Ghorbani, H. Mokarami Ghartavol, Corrosion inhibition of mild steel with tolyltriazole, Mater. Res. 24 (2021) e20200395.

[13] M. Scendo, J. Malyszko, The influence of benzotriazole and tolyltriazole on the copper electrodeposition on polycrystalline platinum from acidic chloride solutions, J. Electrochem. Soc. 147 (2000) 1758–1762.

[14] H. Yan, X. Niu, F. Luo, M. Qu, N. Zhan, J. Liu, Y. Zou, Surface corrosion inhibition effect and action mechanism analysis of 5-methyl-benzotriazole on cobalt-based copper film chemical mechanical polishing for GLSI, ECS J. Solid State Sci. Technol. 12 (2023) 044007, https://doi.org/10.1149/2162-8777/ACCD99.

[15] F. Grillo, D.W. Tee, S.M. Francis, H. Früchtl, N.V. Richardson, Initial stages of benzotriazole adsorption on the Cu(111) surface, Nanoscale 5 (2013) 5269–5273, https://doi.org/10.1039/c3nr00724c.

[16] F. Grillo, D.W. Tee, S.M. Francis, H.A. Früchtl, N.V. Richardson, Passivation of copper: benzotriazole films on Cu(111), J. Phys. Chem. C 118 (2014) 8667–8675, https://doi.org/10.1021/jp411482e.

[17] M. Turano, M. Walker, F. Grillo, C. Gattinoni, J. Edmondson, O. Adesida, G. Hunt, P. Kirkman, N.V. Richardson, C.J. Baddeley, A. Michaelides, G. Costantini, Understanding the interaction of organic corrosion inhibitors with copper at the molecular scale: Benzotriazole on Cu(110), Appl. Surf. Sci. 570 (2021) 151206, https://doi.org/10.1016/j.apsusc.2021.151206.

[18] M. Turano, M. Walker, F. Grillo, C. Gattinoni, G. Hunt, P. Kirkman, N. V. Richardson, C.J. Baddeley, G. Costantini, Adsorption of the prototypical organic corrosion inhibitor benzotriazole on the Cu(100) surface, Corros. Sci. 207 (2022) 110589, https://doi.org/10.1016/j.corsci.2022.110589.

[19] D. Chadwick, T. Hashemi, Benzotriazole adsorption on copper studied by X-ray photoelectron spectroscopy, J. Electron Spectrosc. Relat. Phenom. 10 (1977) 79–83, https://doi.org/10.1016/0368-2048(77)85005-6.

[20] F. Grillo, C. Gattinoni, C.R. Larrea, P. Lacovig, N.V. Richardson, Copper adatoms mediated adsorption of benzotriazole on a gold substrate, Appl. Surf. Sci. 600 (2022) 154087, https://doi.org/10.1016/j.apsusc.2022.154087.

[21] F. Grillo, D. Batchelor, C.R. Larrea, S.M. Francis, P. Lacovig, N.V. Richardson, On-surface condensation of low-dimensional benzotriazole-copper assemblies, Nanoscale 11 (2019) 13017–13031, https://doi.org/10.1039/c9nr04152d.

[22] A. Mirarco, S.M. Francis, C.J. Baddeley, A. Glisenti, F. Grillo, Effect of the pH in the growth of benzotriazole model layers at realistic environmental conditions, Corros. Sci. 143 (2018) 107–115, https://doi.org/10.1016/j.corsci.2018.08.008.

[23] S. Peljhan, A. Kokalj, DFT study of gas-phase adsorption of benzotriazole on Cu (111), Cu(100), Cu(110), and low coordinated defects thereon, Phys. Chem. Chem. Phys. 13 (2011) 20408–20417, https://doi.org/10.1039/C1CP21873E.

[24] C. Gattinoni, P. Tsaousis, C. Euaruksakul, R. Price, D.A. Duncan, T. Pascal, D. Prendergast, G. Held, A. Michaelides, Adsorption behavior of organic molecules: a study of benzotriazole on Cu(111) with spectroscopic and theoretical methods, Langmuir 35 (2019) 882–893, https://doi.org/10.1021/acs.langmuir.8b03528.

[25] C. Gattinoni, A. Michaelides, Understanding corrosion inhibition with van der Waals DFT methods: the case of benzotriazole, Faraday Discuss. 180 (2015) 439–458, https://doi.org/10.1039/c4fd00273c.

[26] M.R. Choudhury, R.D. Vidic, D.A. Dzombak, Inhibition of copper corrosion by tolyltriazole in cooling systems using treated municipal wastewater as makeup water, Arabian J. Sci. Eng. 39 (2014) 7741–7749, https://doi.org/10.1007/s13369-014-1385-z.

[27] F. Grillo, R. Megginson, J. Christie, S.M. Francis, N.V. Richardson, C.J. Baddeley, Structure and reactivity of Cu-doped Au(111) surfaces, e-J, Surf. Sci. Nanotechnol. 16 (2018) 163–171, https://doi.org/10.1380/ejssnt.2018.163.

[28] F. Grillo, J.A. Garrido Torres, M.J. Treanor, C.R. Larrea, J.P. Götze, P. Lacovig, H. A. Früchtl, R. Schaub, N.V. Richardson, Two-dimensional self-assembly of benzotriazole on an inert substrate, Nanoscale 8 (2016) 9167–9177, https://doi.org/10.1039/c6nr00821f.

[29] B. Warren, G.J. Hunt, M. Bryant, A. Neville, A. Morina, M. Gahagan, Automatic transmission fluid corrosion inhibitor interactions with copper, Lubr. Sci. 30 (2018) 301–315, https://doi.org/10.1002/ls.1422.

[30] E.S. Lower, Speciality corrosion inhibitors, Anti-Corros. Methods Mater. 42 (1995) 23–27, https://doi.org/10.1108/eb007378.

[31] G.J. Hunt, R. Javaid, J. Simon, M. Peplow, C. Prengaman, Understanding conductive layer deposits: test method development for lubricant performance testing for hybrid and electric vehicle applications, SAE Int. J. Elect. Veh. 12 (2022), https://doi.org/10.4271/14-12-02-0014.

[32] G.J. Hunt, L. Choo, T. Newcomb, 100 Years of corrosion testing-is it time to move beyond the ASTM D130? the wire corrosion and conductive deposit tests, SAE Int. J. Fuels Lubr. 17 (2023), https://doi.org/10.4271/04-17-01-0002.

[33] N. Fairley, V. Fernandez, M. Richard-Plouet, C. Guillot-Deudon, J. Walton, E. Smith, D. Flahaut, M. Greiner, M. Biesinger, S. Tougaard, D. Morgan, J. Baltrusaitis, Systematic and collaborative approach to problem solving using X-ray photoelectron spectroscopy, Appl. Surf. Sci. Adv. 5 (2021) 100112, https://doi.org/10.1016/j.apsadv.2021.100112.

[34] M.C. Biesinger, B.P. Payne, B.R. Hart, A.P. Grosvenor, N.S. McIntryre, L.W.M. Lau, R.S.C. Smart, Quantitative chemical state XPS analysis of first row transition metals, oxides and hydroxides, J. Phys.: Conf. Ser. 100 (2008) 012025, https://doi.org/10.1088/1742-6596/100/1/012025.

[35] M.C. Biesinger, Advanced analysis of copper X-ray photoelectron spectra, Surf. Interface Anal. 49 (2017) 1325–1334, https://doi.org/10.1002/sia.6239.

[36] NIST X-ray Photoelectron Spectroscopy Database, NIST Standard Reference Database Number 20, National Institute of Standards and Technology, Gaithersburg MD, 20899 (2000), doi: https://dx.doi.org/10.18434/T4T88K (Retrieved Feb 2024).

[37] J.F. Moulder, W.F. Stickle, P.E. Sobol, K.D. Bomben, Handbook of X-ray Photoelectron Spectroscopy, Perkin-Elmer Corporation Physical Electronics Division, Eden Prairie, MN, 1992.

[38] D. Tahir, S. Tougaard, Electronic and optical properties of Cu, CuO and Cu2O studied by electron spectroscopy, J. Phys.: Condens. Matter 24 (2012) 175002, https://doi.org/10.1088/0953-8984/24/17/175002.

[39] K. Wippermann, J.W. Schultze, R. Kessel, J. Penninger, The inhibition of zinc corrosion by bisaminotriazole and other triazole derivatives, Corros. Sci. 32 (1991) 205–230, https://doi.org/10.1016/0010-938X(91)90044-P.

[40] T. Kosec, D.K. Merl, I. Milošev, Impedance and XPS study of benzotriazole films formed on copper, copper–zinc alloys and zinc in chloride solution, Corros. Sci. 50 (2008) 1987–1997, https://doi.org/10.1016/J.CORSCI.2008.04.016.

[41] M. Saavedra-Torres, C.A. Escobar, F. Ocayo, F. Tielens, J.C. Santos, 1,2,3-Benzotriazole derivatives adsorption on Cu(1 1 1) surface: A DFT study, Chem. Phys. Lett. 689 (2017) 128–134, https://doi.org/10.1016/J.CPLETT.2017.09.067.

[42] A. Kokalj, S. Peljhan, M. Finšgar, I. Milošev, What determines the inhibition effectiveness of ATA, BTAH, and BTAOH corrosion inhibitors on copper? J. Am. Chem. Soc. 132 (2010) 16657–16668, https://doi.org/10.1021/ja107704y.

[43] A. Kokalj, N. Kovačević, S. Peljhan, M. Finšgar, A. Lesar, I. Milošev, Triazole, benzotriazole, and naphthotriazole as copper corrosion inhibitors: I. Molecular electronic and adsorption properties, ChemPhysChem 12 (2011) 3547–3555, https://doi.org/10.1002/CPHC.201100537.

[44] A. Kokalj, S. Peljhan, Density functional theory study of ATA, BTAH, and BTAOH as copper corrosion inhibitors: adsorption onto Cu(111) from gas phase, Langmuir 26 (2010) 14582–14593, https://doi.org/10.1021/la1019789.

[45] X. Xu, A. Zuo, S. Liu, Y. Tang, DFT study on the adsorption of 1H-benzotriazole on the (1 1 1) surface of modelled Cu–25%Zn brass, Mater. Chem. Phys. 312 (2024) 128683, https://doi.org/10.1016/J.MATCHEMPHYS.2023.128683.

[46] F. Li, Z. Wang, Y. Jiang, C. Li, S. Sun, S. Chen, S. Hu, DFT study on the adsorption of deprotonated benzotriazole on the defective copper surfaces, Corros. Sci. 186 (2021) 109458, https://doi.org/10.1016/J.CORSCI.2021.109458.

[47] R. Walker, Oxidation behaviour up to 500°C of tin bronze pretreated with benzotriazole, Br. Corros. J. 34 (1999) 304–309, https://doi.org/10.1179/000705999101500914.

[48] X. Chen, H. Häkkinen, Divide and protect: passivating Cu(111) by Cu-(benzotriazole) 2, J. Phys. Chem. C 116 (2012) 22346–22349, https://doi.org/10.1021/jp3055894.

[49] Y. Ling, Y. Guan, K.N. Han, Corrosion inhibition of copper with benzotriazole and other organic surfactants, Corrosion 51 (1995) 367–375, https://doi.org/10.5006/1.3293601.